Electrical Stimulus-Based Characterization for Calibration and Testing of MEMS Accelerometer and Gyroscope

by

Lingfei Deng

A Thesis Presented in Partial Fulfillment
of the Requirements for the Degree
Master of Science

Approved July 2012 by the
Graduate Supervisory Committee:

Sule Ozev, Chair
Hongyu Yu
Jennifer Blain Christen

ARIZONA STATE UNIVERSITY

August 2012

ABSTRACT

Micro-Electro Mechanical System (MEMS) is the micro-scale technology applying on various fields. Traditional testing strategy of MEMS requires physical stimulus, which leads to high cost specified equipment. Also there are a large number of wafer-level measurements for MEMS. A method of estimation calibration coefficient only by electrical stimulus based wafer level measurements is included in the thesis. Moreover, a statistical technique is introduced that can reduce the number of wafer level measurements, meanwhile obtaining an accurate estimate of unmeasured parameters. To improve estimation accuracy, outlier analysis is the effective technique and merged in the test flow. Besides, an algorithm for optimizing test set is included, also providing numerical estimated prediction error.

ACKNOWLEDGMENTS

I wish to thank my advisor Dr. Sule Ozev for the support and help on this research project, as well as my committee members. I am also pleased to have this opportunity to thank my colleagues, Vinay Kundar, Naveen Jangala Naga, Ender Yilmaz for all of the help.

Finally, I would like to thank my parents, for their patience, support, encouragement.

TABLE OF CONTENTS

Page

LIST OF TABLES..v

LIST OF FIGURES..vi

CHAPTER

INTRODUCTION..1

1.1 Micro-Electron Mechanical System...1

1.2 Capacitive MEMS Accelerometer...2

1.2.1 Capacitive MEMS Accelerometer Structure.......................2

1.2.2 Capacitive MEMS Gyroscope Structure............................6

1.3 Research Goal..9

2 RELATED WORK..15

3 BACKGROUND...21

3.1 Statistical Framework...21

3.1.1 Kernel Based Estimation...22

3.2 Defects and Outliers...27

3.2.1 Multi-D Outlier Analysis..27

3.2.2 Algorithm Flow..29

CHAPTER Page

4 PARAMETER ESTIMATION AND TEST SELECTION......................30

4.1 Statistical Learning Phase...31

4.1.1 Determining Reduced Set of

Tests for Outlier Detection..32

4.2 Selection of Tests to Increase Estimate Accuracy.......................34

5 A CASE STUDY: ACCELEROMETER...38

5.1 Determining Dynamic Accelerometer Measurements for

Correlating to Calibration Coefficients...............................38

5.2 Simulation Results…………………………………………..41

6 A CASE STUDY: GYROSCOPE...46

6.1 Outlier Analysis on Full Set of Measurements...........................46

6.2 Outlier Analysis based on Subset of Measurements...................48

6.3 Verification sets consistency analysis..47

6.4 Experimental Results of Estimation Process ..…………………..51

5 CONCLUSION AND FUTURE WORK..56

REFERENCE..58

LIST OF TABLES

Table Page

5.1 RMS errors after each test with different training size..................................45

6.1 Training set size impact on outlier identifying...48

6.2 set size impact on identifying outliers not using all dimensions...................49

6.3 Improvement on estimation accuracy after outlier screening........................52

LIST OF FIGURES

Figure Page

1.1 Basic Capacitive MEMS structure..3

1.2 Accelerometer structure with acceleration..4

1.3 Simplified on-chip implementation of accelerometer structure.......................6

1.4 Simplified vibrating gyroscope model...8

1.5 Gyroscope sensing and driving structure...9

3.1 Flow chart of parameter estimation...25

3.2 Two-dimension parameter estimation..26

3.3 Parameter are localized after two measurements...26

4.1 Generic estimation test flow..31

4.2 Identifying outlier using subset of all dimensions……………………………..33

4.3 Algorithm for finding test list *{i}*....……………………………………….37

5.1 Complete estimation test flow..41

5.2 Training set distance histogram plot..………………….....……………………..42

5.3 Calibration Coefficient is localized after 2 tests...43

5.4 Scatter plot of Real vs Estimate after all tests...44

6.1 Outlier percentage *vs* index of simulations..47

6.2 Average RMS errors after different number of tests for

4 different verification set (a), (b), (c), (d)..50

Figure Page

6.3 Experimental results of RMS errors using different number of tests..............51

6.4 Measurement ten is localized after tests on whole test list.............................53

6.5 Estimated measurements are localized after all of the tests............................54

6.6 Worst and best estimated devices during prediction process..........................55

INTRODUCTION

1.1 Micro-Electron Mechanical Systems

Micro-Electron Mechanical Systems (MEMS) transfer a mechanical stimulus to an electrical response. It is a fast growing field in the silicon industry. Yole Development report [1] indicates that the MEMS device market was $3.84 billion in 2003 and according to the iSuppli market analysis [2], the MEMS market reached around $7 billion in 2011. There are various MEMS applications used in automotive, health care, military, aerospace, and portable electronics domains. For instance, in the automotive industry, accelerometers are used for airbags; pressure sensors are used for monitoring the engine and tire pressure; and gyroscopes are used for navigation and control. In the electronics industry, accelerometers and gyroscopes are used for gravity and motion sensing, and pressure sensors are used for touch sensing. In the health care industry, MEMS can also be utilized for sensing blood pressure, detecting motion, and measuring forces. Overall, the MEMS technology is widely utilized in our daily life, providing convenience, entertainment, health care, and safety.

1.2 Capacitive MEMS sensors

Berkley Sensor and Actuator Center at University of California developed the first MEMS actuator in 1988 [3]. Low fabrication costs and higher performance make MEMS sensors good candidates for silicon integration [4]. MEMS sensors have a simple structure and better precision with some additional benefits in comparison to conventional sensors, such as the conventional piezoelectric accelerometers used in vibration measurements [5]. MEMS accelerometer can be manufactured with 10% of cost of the cheapest conventional accelerometer. The small size of MEMS sensors is a significant advantage, in that, it prevents intrusion of the system where MEMS sensors are used. For example, inertial properties can be measured without adding mass, and fluid properties can be measured without disturbing the fluid significantly. Besides low fabrication cost, low power consumption and high signal integration density are also the benefits of MEMS sensors.

1.2.1 Capacitive MEMS Accelerometer Structure

A typical MEMS accelerometer structure is shown in Figure 1.1. The Movable shuttle M is connected by two springs with the spring constant, K. Two fixed plates, together with the movable plate, form two capacitors $C1$ and $C2$. If there is no acceleration and no stationary capacitance offset, the movable

plate is at the center of two fixed plates, so that both $C1$ and $C2$ has the same capacitance value:

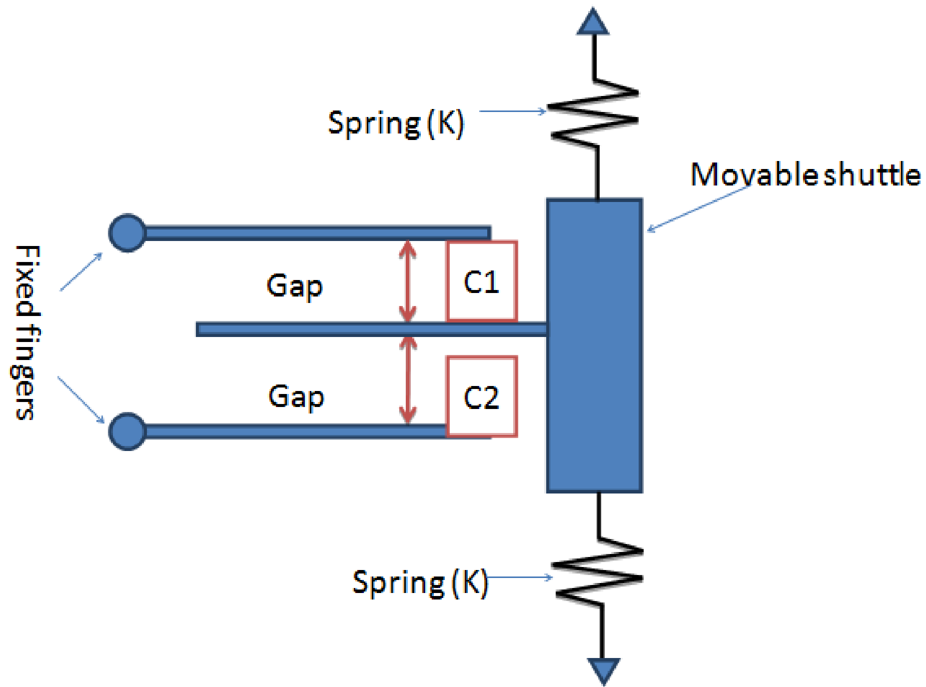

Figure 1.1 Basic Capacitive MEMS structure

$$C1 = C2 = \frac{\xi_o \xi A}{d} \qquad (1.2.1)$$

where ξ_o is the vacuum dielectric constant, ξ is relative dielectric constant, A is the overlap area between movable and fixed plates, and d is the gap between them.

If a vertical acceleration is applied to this system, as shown in Figure 1.2, the MEMS accelerometer will be activated by this stimulus which contributes to a certain amount of small displacement of x, then, $C1$ and $C2$ will be

$$C1 = \frac{\xi_o \xi A}{(d-x)} \tag{1.2.2}$$

$$C2 = \frac{\xi_o \xi A}{(d+x)} \tag{1.2.3}$$

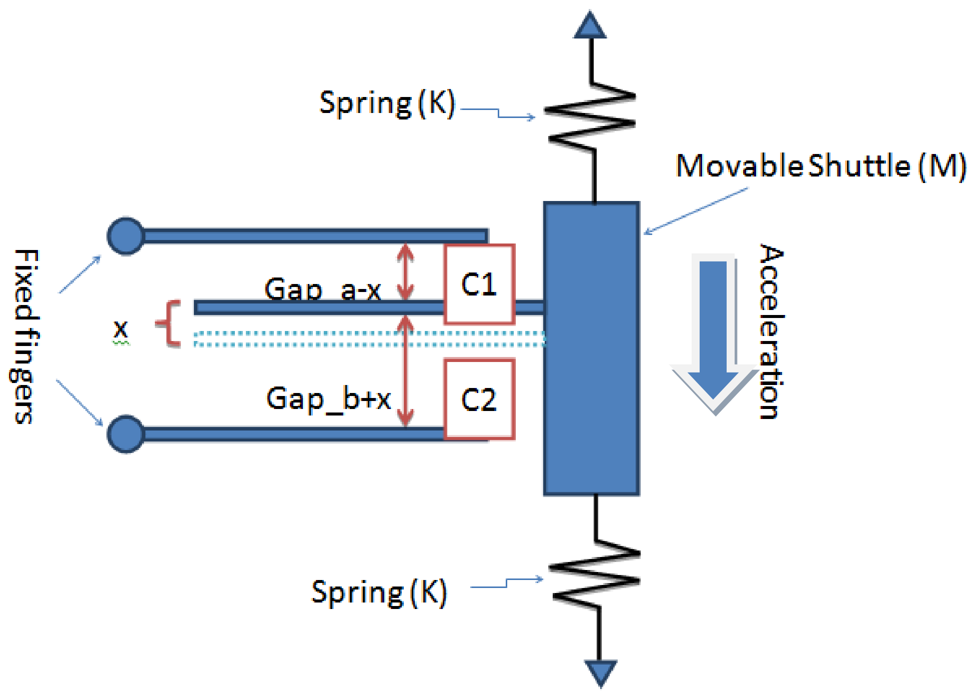

Figure 1.2 Accelerometer structure with acceleration

Let us define

$$2\Delta C = C1 - C2 = 2\xi_o \xi A \frac{x}{d^2 - x^2} \tag{1.2.4}$$

By resolving equation (1.2.4), for small displacement x, x is approximately linearly related to ΔC:

$$x \approx \frac{d^2}{\xi_o \xi A} \Delta C \tag{1.2.5}$$

For the spring-mass system, the acceleration a is:

$$a = \frac{k}{m} * x \tag{1.2.6}$$

Combining equations (1.1.5) and (1.1.6)

$$a = \frac{d^2}{\xi_o \xi A} \Delta C \tag{1.2.7}$$

Hence, the mechanic property a is linearly transferred to electrical property ΔC. In other words, ΔC is the linear transducer from mechanical property to electrical property. Figure 1.3 shows simplified on-chip implementation of a MEMS accelerometer. There are various sensing fingers as well as the comb-drive fingers. Comb-drive fingers are used for generating electrostatic force to mimic acceleration for self-test purposes.

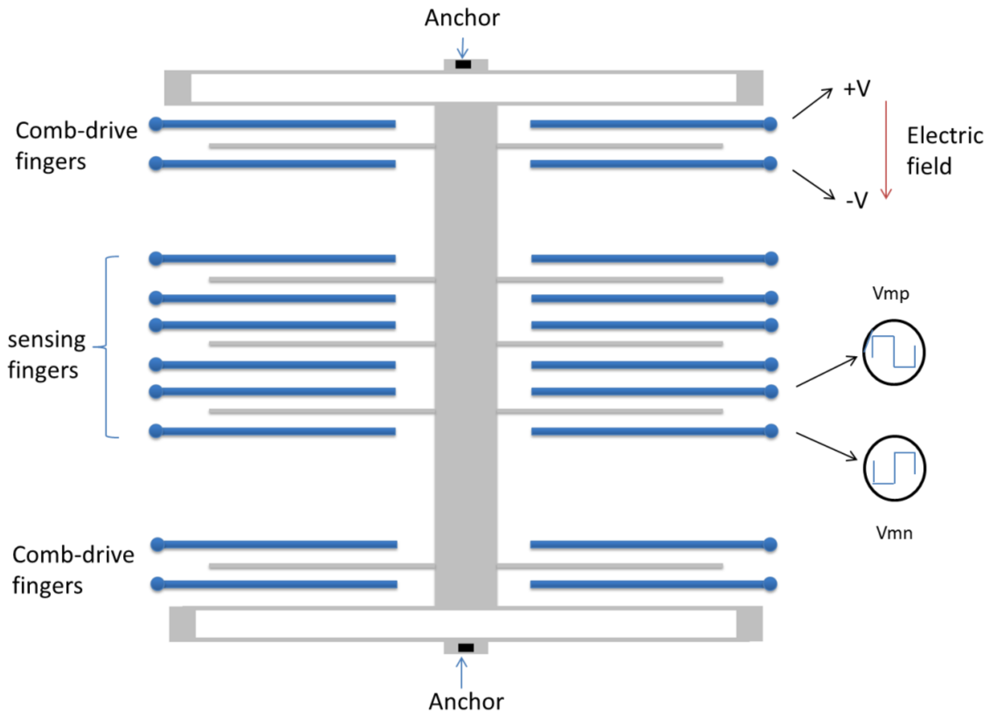

Figure 1.3 Simplified on-chip implementation of accelerometer structure

1.2.2 Capacitive MEMS Gyroscope Structure

The majority of MEMS gyroscopes use the vibrating beam structure. Figure 1.4 is the simplified vibrating MEMS gyroscope model. It is in the x-y domain with z axis angular velocity. If proof mass has a velocity in x axis, y axis will generate Coriolis force. Equation (1.3.1) presents the vector relationship of x axis Coriolis acceleration. The Vibrating gyroscope makes an x-axis oscillation at x axis resonant frequency ω_{ox}, and y axis would also oscillate at this frequency due to Coriolis force. However, the y axis vibrating phase shift depends on the

ratio of k_d and k_s [6]. If the ratio is 1, phase shift is 90 degrees, which is desired for demodulation. If the x axis resonator oscillates as Equation (1.3.2), the y axis resonator behaves as Equation (1.3.3), where G is the ratio of k_d and k_s, Q_y is the quality factor of x axis resonator, ω_z is z axis rotation velocity and ω_{ox} is x axis resonant frequency. ϕ is shown in Equation (1.3.4).

$$\vec{a} = -2\vec{\omega} \times \vec{v} \tag{1.3.1}$$

$$x(t) = A_x \sin(\omega_{ox} t) \tag{1.3.2}$$

$$y(t) = -\frac{2A_x\omega_z}{\omega_{ox}\sqrt{(G^2-1)^2 + G^2/Q_y{}^2}}\cos(\omega_{ox}t + \phi) \tag{1.3.3}$$

$$\phi = \arctan\frac{G}{(1-G^2)Q_y} \tag{1.3.4}$$

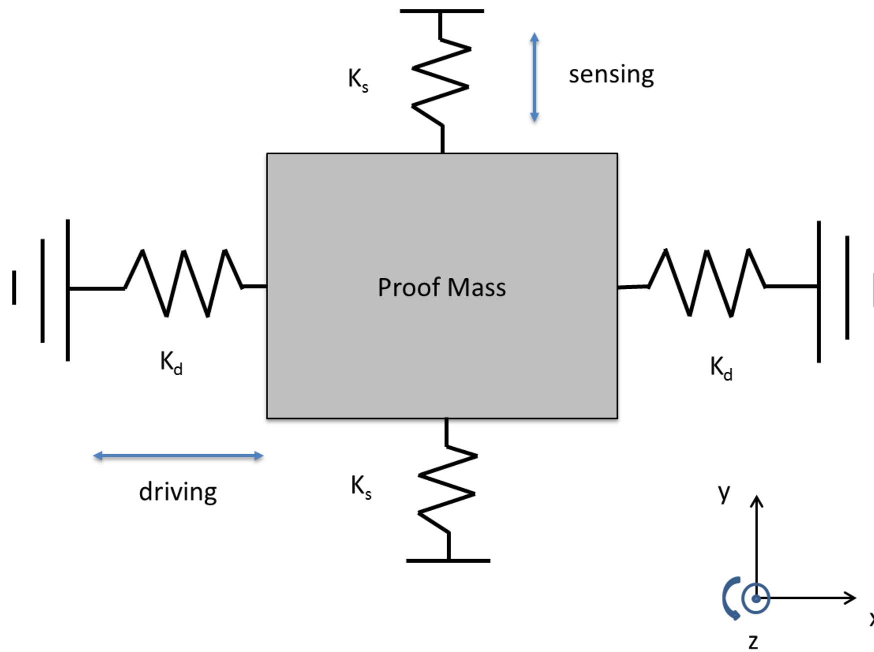

Figure 1.4 Simplified vibrating gyroscope model

Figure 1.5 demonstrates simplified on-chip implementation of MEMS gyroscope. The Comb-drive fingers generate electrostatic force to drive the proof mass oscillating at the x axis. The proof mass would also oscillate at the same frequency at the y axis if there is a z axis angular velocity ω_z. According to equation (1.3.3), the y axis acceleration which is a function of ω_z could be measured by the y axis accelerometer. Then, the angular velocity could be detected by measuring the y axis acceleration.

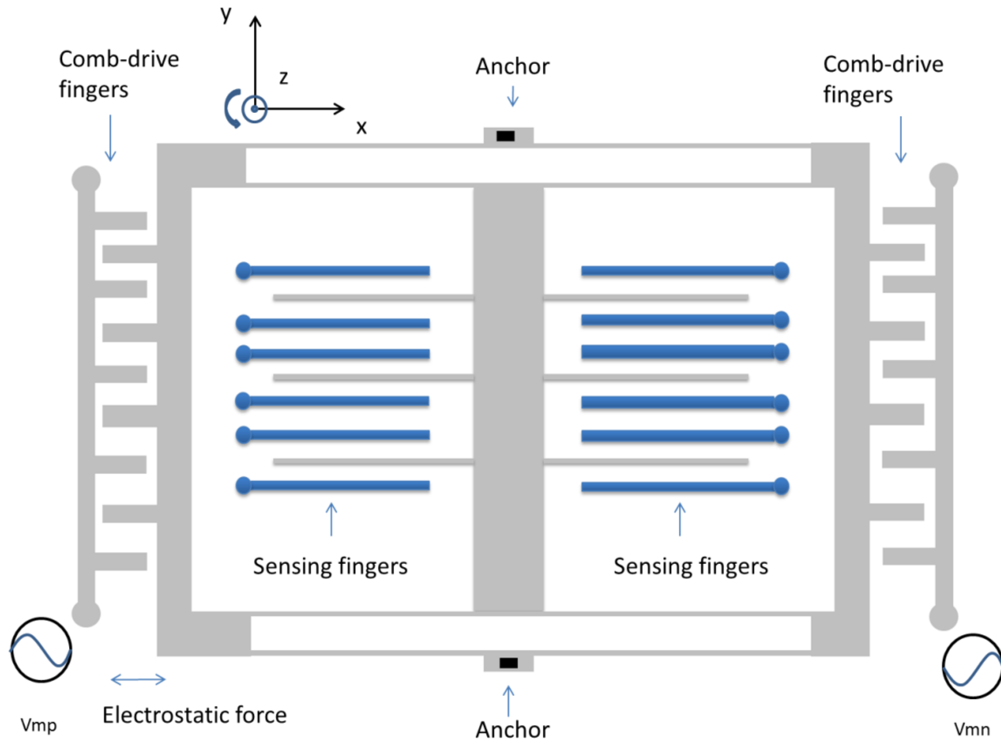

Figure 1.5 Gyroscope sensing and driving structure

1.3 Research Goals

MEMS devices convert a physical stimulus to an electrical response, which can then be measured with electronic circuitry and the attributes of the physical stimulus can be obtained using mathematical relations. For instance, in the case of the accelerometer, the measured quantity is the capacitance, or the difference of the two capacitances, and Equation (1.2.7) can be used to convert this information to acceleration, which is the actual measurement goal. However, the accuracy of this information depends on two factors: (a) measurement

accuracy of the capacitance difference, and (b) knowledge on the parameters of the internal MEMS structure. To enhance the accuracy of the capacitance measurements, many circuit-level techniques can be applied, such as correlated double sampling and chopper stabilization. Multiple sense fingers can be used, the measurements can be repeated multiple times, and the sensitivity can be increased to 155mV/fF [7] or 300mV/fF [8].

In contrast, the internal parameters of the MEMS structure, permittivity, mass, and spring constant, cannot be directly measured. As with any manufacturing process, these parameters are subject to process variations. After manufacturing, the only information that is available is the nominal value of these parameters.

In order to facilitate accurate readings from the MEMS devices, it is essential that these devices are calibrated. Moreover, similar to any other manufacturing process, MEMS devices are subject to manufacturing defects, which alter the complete structure and result in loss of functionality or shift in the internal parameters of the device. In order to prevent any defective device from being shipped to the customer, these devices also need to be tested for manufacturing defects.

Testing and calibration of MEMS devices is an important component of the overall manufacturing cost. In order to obtain calibration parameters, these

devices need to be excited with physical stimulus, which requires specialized, expensive equipment. Moreover, in order to prevent defective devices from being integrated with functional ASICs, MEMS devices need to be dynamically tested at the wafer-level, requiring a large number of dynamic measurements, which increases the test time, and results in high test cost.

During the MEMS product testing, there are two phases. The first phase is the wafer level testing that includes two types: simple structural tests and dynamic measurements. Simple structural tests, such as continuity tests, and DC tests, are currently in use in the industry. The main goal is to eliminate defective MEMS dies to save costs associated with packaging and/or ASICs that go along with them. Dynamic measurements are currently used in a limited capacity in the industry. Greater use of dynamic measurements is desired not only to eliminate defective MEMS devices but also to enable a detailed characterization at the wafer-level. Examples of dynamic measurements include frequency-dependent characteristics such as resonant frequency, damping factor, poles and zeros.

The second phase of testing occurs after packaging where the goal is to evaluate the full MEMS system functionality and performance. Due to process variations, the MEMS response varies, calibration parameters in terms of coefficients that relate the actual response to the desired response are determined in this phase. Characterization and calibration of MEMS devices require

specialized, high cost testing equipment such as high-gravity shakers (up to 40gravity). Hence, one current research and industry direction is to use dynamic wafer level measurements to determine calibration coefficients without resorting to expensive physical stimulus based test equipment.

However, in order to determine these calibration coefficients without physical stimuli, a large number of wafer-level parameters may need to be measured. Most of these dynamic parameters are in the low-frequency domain and require long test times. This shifts the cost burden of MEMS characterization and calibration from equipment cost of physical stimulus to test time cost using electrical characterization. Fortunately, most of these dynamic parameters are correlated. Measuring all of them is therefore typically unnecessary. It is desirable to measure a subset of these parameters while still obtaining a reasonably accurate estimate of the unmeasured parameters.

To summarize, there are two challenges in the realm of testing and calibration of MEMS devices: (a) determining electrical measurements that can replace physical excitation, and (b) reducing the number of such measurements to reduce the overall test time.

This thesis aims at lowering the production cost of MEMS devices by addressing these test challenges. Specifically, the aim of the thesis work is to develop a unified framework for characterization, testing, and calibration of

MEMS devices using a reduced number of electrical measurements, thereby eliminating the need for physical stimulus as well as reducing the overall test time, thereby reducing the test cost.

In order to achieve these goals, a statistical modeling framework is used to facilitate the mapping between various types of information. This common statistical framework is first used to map the reduced number of electrical measurements to the full set of measurements. An outlier analysis technique based on this statistical framework is developed to identify potentially defective MEMS devices during wafer-level testing, thereby preventing their packaging with functional ASICs. The statistical mapping technique is also used to correlate the information obtained from dynamic wafer-level measurements to final calibration coefficients, thereby eliminating the need for physical stimulus.

Since every MEMS device behaves in a slightly different fashion, two capacitive MEMS devices have been selected as targets for this study. The first is an accelerometer, and the second is a gyroscope. The accelerometer has been selected to demonstrate that it is possible to define electrical tests that can correlate well with the internal device parameters and hence the final calibration coefficients. The gyroscope has been selected to demonstrate that it is possible to reduce the number of measurements without compromising the accuracy of the information that has been obtained by the testing process.

To summarize, the goals of this thesis are:

- Determining electrical measurements for the estimation of calibration coefficient for the MEMS accelerometer
- Multidimensional outlier analysis to detect and eliminate defective devices
- Determining an optimal subset of wafer-level measurements for the gyroscope to reduce test time

CHAPTER 2. RELATED WORK

Over the past several decades, many testing and calibration methodologies have been proposed for the MEMS sensors.

Some of the methodologies focus on the mechanical faults detection. In [9], the authors characterize contamination fault behavior of a MEMS resonator. They develop a process simulator with the contamination fault injection and a mechanical simulator generating mechanical parameters (resonant frequency and spring constant). From the simulation results, the contamination defects contribute to various defective structures which result in a variety of faulty behaviors. In [10], the testing of the MEMS flow sensor and the optical sensor have been discussed, including the customized ATE and a test setup for detecting the faults (misalignment of the flow sensor, voids in the waveguide of the optical sensor). In [11], the faults caused by micro-machining defects have been targeted. A circuit level approach is used to model the behavior of MEMS sensors (thermal MEMS and capacitive resonator), as well as the fault behavior. Specifically, thermal shorts are used to model the realistic fault behavior for the thermal MEMS; a circuit level decomposition for the resonator is required to inject the faults like broken fingers. According to the simulation results, the tests response can effectively reveal the faults.

Some of the methodologies have paid more attention on achieving the electrical-only test setup, for self-test purpose and elimination of the expensive mechanical ATE. For example, solutions for three types of MEMS have been proposed in [12]. The capacitive accelerometer utilizes electrostatic force from comb-drive fingers, while the piezo-resistive sensors and the thermopile based sensors use heat from the heating resistor. Regarding the BIST solution, [13] introduces a dual-mode BIST technique for the capacitive MEMS devices. Capacitor partitioning of fixed capacitance plates enables the operation of different BIST modes for symmetry and sensitivity tests. In addition, defects such as stiction and finger height mismatch can be effectively detected by the symmetry and sensitivity tests response. [14] and [15] use the impulse response evaluation technique to implement BIST response to the digital domain. They both use polynomial linear feedback shift register (LFSR) based pseudo-random test sequence. The test approach is achieved by implementing a DAC and an ADC between the MEMS sensor, converting the MEMS sensor in digital domain. Then, according to the input stimulus and the output response, a correlator will generate the signature set for classification of faulty or normal devices. Specifically, in [15], Maximum-Length Sequences (MLS) is used to generate the input sequences in the noisy environment. A general resonator is exemplified in [14], with a decent test length and 100% fault coverage. Meanwhile, the case study of cantilevers and

the bridge is presented in [15], indicating that over 20dB improvement for signal can be achieved by using MLS technique.

Some MEMS test methodologies focus on the ATE equipment. A tester architecture has been proposed for the MEMS testing and calibration [16]. By moving some of the tester intelligence from the electrical stimuli part to the physical stimuli part, the proposed architecture is able to reduce the number of internal wires, at the same time, increase the parallelism rate and reduce the test time. An accelerometer case study indicates test time can be reduced to less than 10% of the test time with the conventional architecture. [17] demonstrates the necessity of high gravity tester. The acceleration level for the testing of MEMS applications should be in the tens of thousands of gravity. Therefore, five specified testers have been proposed to achieve that level, which are hammer blow, Hopkinson bar, piezo actuators, free fall drop and half sine shock.

The author of [18] considered the non-ideality in the gyroscope testing process. The test error by a large coupled misalignment angle is concentrated. An uncoupling technique, aiming at uncoupling misalignment angle and scale factor, has been proposed to make the testing of gyroscope immune to misalignment angle. In addition, a designed tester has been also proposed to verify the effectiveness by the experimental results.

Another trend of MEMS testing and calibration is to use a statistical framework for test compaction, parameter prediction, and calibration.

A two-class support vector machine (SVM) is used in [19] for the specification test compaction of analog circuits and MEMS. Based on the data of a training set, the two-class vector is able to pass or fail the device when it goes through a pruned test set. In addition, a guard-band region is defined and used to improve yield loss and defect escape, by applying further tests on devices falling in guard-band region. An example of the accelerometer testing indicates this technique achieves 0.2% defect escape and 0.1% yield loss.

Multivariate adaptive regression splines (MARS) is used in [20] for the prediction of the capacitive accelerometer parameters, such as proof mass, spring constant, and damping coefficient. An input-frequency searching algorithm (gradient-search) has been proposed to select the single tone and three-tone frequencies, from which the output responses are highly correlated to mechanic parameters. As a result, a decent estimate is achieved.

MARS model is also used in [21]-[23] for the test and calibration of the convective accelerometer. In addition, wafer-level tests are emphasized due to the reduction of packaging cost. In [21], simple measurements with an easily-implemented electrical setup are defined and most parametric faults can be detected with them. In [22] and [23], a MARS model and an electrical

measurement are used to calibrate the convective accelerometer. This measurement is easily setup and highly correlated to device sensitivity. Depending on the tolerance limits, tradeoffs have been evaluated considering fault coverage, yield loss and test efficiency.

Artificial Neural Networks (ANN) are also one of the regression-based models, used in [24] for the testing and diagnosis of MEMS pressure sensors. The MEMS sensor is treated as a black-box, and modeled as Lumped-C by the ANN. After the fault injection on the readout circuits and the MEMS sensor, the electrical response is mapped to a fault.

A specified testing and calibration method has been proposed in [25] for MEMS capacitive accelerometers. This method concentrates on mathematical relations between the sensitivity and process parameters. Although process parameters are not accessible in the actual testing phase, this method initializes process parameters the following two ways: the first is assigning these parameters the nominal process value, and the second is based on the experimental characterization of the sensitivity of a small training set. In addition, a fully electrical test setup includes resonant frequency, pull-in voltage, and the sensitivity of the driving voltage. Moreover, parametric faults are injected in process parameters, including global variations and local mismatches. Results have shown the potential of this method.

This thesis also concentrates on the statistical models and mapping techniques for the testing and calibration of MEMS devices. However, different from [21]-[24], kernel-based statistical framework is employed due to its capability of handling large dimensionality and obtaining reasonable estimation accuracy. In addition, the test set compaction is also included, but in comparison to [19], unmeasured parameters are necessary to be reasonably estimated. Moreover, defects and outliers, which behave randomly, remarkably corrupt the statistical learning and destroy the estimation accuracy. In this thesis, a technique of a reduced test set for outlier screening prevents outliers and defects in both the learning and the testing phase. Furthermore, in order to eliminate physical testers, the tests are electrically-only set up at the wafer level, and thus the detected defects can be prevented from being integrated with ASIC; saving packaging cost.

CHAPTER 3. BACKGROUND

3.1 Statistical Framework

The main purpose of this thesis is to reduce the wafer level dynamic measurements, while obtaining a desired estimate on unmeasured parameters, including the unmeasured wafer-level parameters, and the final calibration coefficients. To achieve this goal, statistical mapping techniques are used. This process requires a small set of training devices for deducing correlations among these measurements.

Several aspects of this problem are important in selecting a framework for statistical estimation. First, the framework needs to be able to handle large dimensionality in the statistical modeling as the number of measurements can be large. Second, we wish to obtain a reasonably accurate estimate of the errors that are made during the mapping process. Third, the errors in one step of the process, including measurement errors and estimation errors, need to be propagated to the next step of the process. Finally, the technique should be easily extendable to determine outliers in multiple dimensions and eliminate them from the training step so as to avoid training on defective devices. Kernel-based probability density function modeling satisfies these requirements and is therefore selected as the basis for the statistical framework.

3.1.1 Kernel Based Density Estimation

Kernel based density estimation enables us to build joint probability density function (JPDF) and update JPDF after each measurement. Kernel based estimation has relatively high estimation efficiency in multi-dimensions, even with a small set of data, providing high accuracy [26].

Kernel based probability distribution is defined as in equation (3.1.1) and used in non-parametric estimation techniques. There are several well-known kernel functions, such as uniform, triangular, epanechnikov, biweight, triweight, Gaussian and tricube. Gaussian distribution is selected as kernel due to the large amounts of previous research and analysis.

$$\int_{-\infty}^{\infty} K(x)dx = 1 \qquad (3.1.1)$$

$$p\hat{d}f(s) = \frac{1}{n\prod h_j}\sum_{i=1}^{n}\prod_{j=1}^{M} K\left(\frac{s_j - u_{i,j}}{h_j}\right) \qquad (3.1.2)$$

Equation (3.1.2) presents the probability density function using kernels. i stands for i^{th} device, j represents j^{th} measurement, s_j is the measurement result of the jth measurement. n is the number of training devices, M is the size of measurements. $u_{i,j}$ is the mean value for j^{th} measurement. h_j is the kernel

smoother used for adjusting and fitting the distribution curve. We define the kernel smoother as equation (3.1.3), aiming at minimization of mean integrated squared error (MISE).

$$h_j = \left(\frac{4}{d+2}\right)^{\frac{1}{d+4}} \sigma_j n^{-\frac{1}{d+4}} \tag{3.1.3}$$

where σ_j is the standard deviation of jth measurement parameter and d is the dimension number. Kernel-based probability estimation enables a non-parametric estimation of the JPDF over all parameters. However, our goal is to be able to measure a subset of these parameters, while determining the unmeasured parameters. This JPDF can be used for this purpose since each measurement provides a reference in the multidimensional space, and can be used to localize the rest of the parameters provided that there is some correlation between the measured parameter and the unmeasured parameter.

Figure 3.1 explains the parameter localization process. A small set of training devices are subjected to full measurements in order to collect multi-dimensional statistical correlations to build the JPDF (Equation (3.1.2)). These devices serve as the training set to build the statistical correlations. This information is obtained off-line before the actual testing phase begins.

During the testing phase, each device goes through a reduced set of measurements. The result of each measurement can be used to update the JPDF,

effectively collapsing it in the dimension corresponding to that measurement. The estimated PDF is shown in Equation (3.1.4) and (3.1.5).

$$p\hat{d}\, f(s_k) = \frac{1}{n\prod h_j} \sum_{i=1}^{n} w_i \prod_{j=1}^{M} K\left(\frac{s_{k,j} - u_{i,j}}{h_j}\right) \tag{3.1.4}$$

$$w_i = w_i * \frac{K\left(5 * \frac{S_{i,j} - u_{i,j}}{\sigma_j}\right)}{K(0)} \tag{3.1.5}$$

where w_i is kernel weight, i is the ith device in the actual testing phase, j represents the jth measurement parameter. Initially, all weights w_i are equal before measurements. The JPDF of the ith device is the same as the JPDF built by the training set, because each sample of the JPDF is equally likely. After a reduced set of measurements, the JPDF will be iteratively updated with the new weights: the weights corresponding to the samples close to the conducted measurements are increased whereas the other weights are decreased, as in Equation (3.1.5). Therefore, the JPDF of unmeasured parameters will be updated due to the iteratively updated weights (Equation (3.1.4)). At the end of this iterative process, the updated JPDF represents the estimate of the unmeasured parameters. Using this JPDF, for each unmeasured parameter, it is possible to determine the most likely value as well as a span. The most likely value serves as the estimate of this

unmeasured parameter whereas the span is indicative of the potential error with a 99.9% confidence.

Figure 3.2 is a two-dimension fictitious function example demonstrating this localization process. It is a scatterplot of parameters S1 and S2 for a training set. It is obvious that S1 and S2 are correlated and circled by the red ellipse. The blue curves under two axes are the PDF of S1 and S2 before any tests. After measuring S2, shown as the red arrow, it can be found that S1 parameter has a smaller span located on the right side of the original distribution. In other words, the PDF of S1 is updated and narrowed due to the information on the S2 parameter. The process works in a similar flow for multiple dimensions, by iteratively using information that is obtained from each measurement. Figure 3.3 is an example illustrating how S1 is localized by two measurements. The most likely value moves towards the real value after each test.

Figure 3.1 Flow chart of parameter estimation

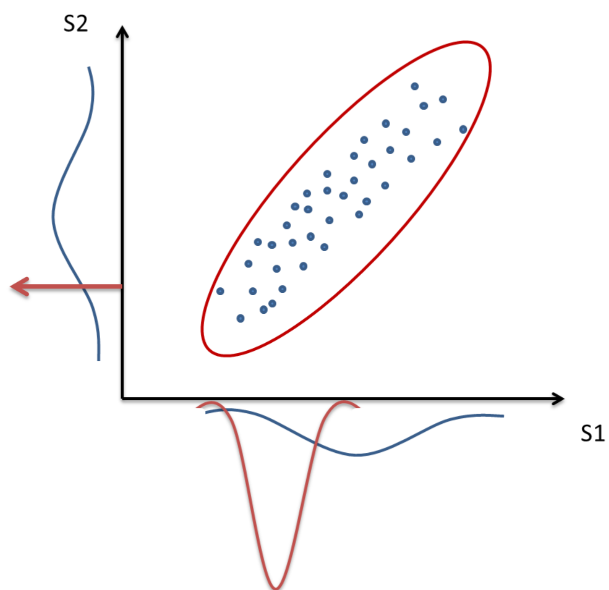

Figure 3.2 Two-dimension parameter estimation

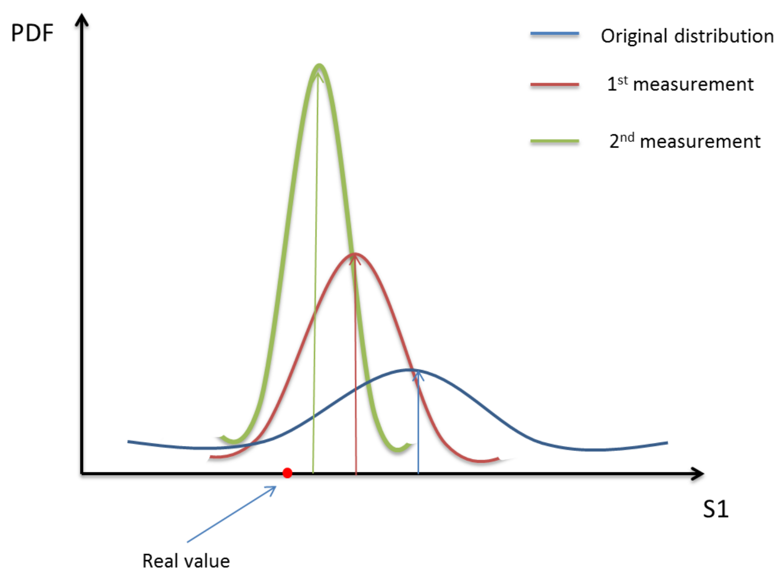

Figure 3.3 Parameter are localized after two measurements

3.2 Defects and Outliers

Outlier devices behave significantly different compared with the bulk of the population. They are generally considered as potentially defective. Defective devices display random behavior. Due to this randomness, they may corrupt the statistical learning process. These outlier devices need to be identified for the training samples so as to prevent them from influencing the learning process. During this step, all test data are available as the training set has the complete measurement results. Outliers also need to be identified during the actual test phase since using responses with the correlations learned from non-outlier devices may result in incorrect results. The challenge in this step is that not all test data are available since we opted for a subset of measurements.

3.2.1 Multi-D Outlier Analysis

One way of simplifying multi-dimensional analysis is to convert to the information in multiple dimensions into one dimension through a set of transformations. If measurement parameters are satisfied as Gaussian distribution, Mahalanobis distance can be employed as a good candidate as shown in Equation (3.2.1):

$$MD^2(s_i) = (s_i - \mu_i)^T C^{-1} (s_i - \mu_i) \tag{3.2.1}$$

where s_i is the measurement parameter of ith device, μ_i is the mean value, C is covariance matrix and $()^T$ is transpose function.

However, nonlinearity of the MEMS device behavior makes distributions much more complicated. Therefore, we need to introduce a nonparametric model and make a definition of distance. Kernel based model is also a good candidate for outlier analysis. The distance of kernel based model is defined as equation (3.2.2) and equation (3.2.3).

$$D_j(s_i) = -\log\{\frac{1}{N}\sum_{k=1}^{N} K_j(\frac{s_{i,j} - \mu_{k,j}}{h_j})\} \tag{3.2.2}$$

$$D_{\{j\}}(s_i) = \sum_{\{j\}} D_j(s_i) \tag{3.2.3}$$

where N is the number of devices in the training set, s_i is the measurements associated with a device whose distance is to be evaluated, $\mu_{k,j}$ is the mean value of kernel sample k for the jth measurement, and h_j is the kernel smoother for the jth measurement. $D_j(s_i)$ is the one dimensional distance metric of the device instance under evaluation and $D_{\{j\}}(s_i)$ is the collective distance that device instance over all measurements [27].

It is difficult to derive statistical distribution of $D_{\{j\}}$ for a nonparametric model. But $D_{\{j\}}$ can be estimated as a Chi-squared distribution [27]. Due to the

fact that $D_{\{j\}}$ is normalized, it is better to assign a boundary and identify those devices as outliers which fall out of boundary.

3.2.2 Algorithm Flow

The proposed outlier analysis technique is based on selecting a small set of training devices, building a distance core, defining a boundary for outlier determination, and finally filtering out all the outliers. First, in order to get a robust statistical model, it would be better to filter out obvious outliers in each dimension in the training set independently. To this end, devices outside the ±6 sigma range are removed. The second step is to calculate the distance metric according to equation (3.2.2) and (3.2.3), as well as define a boundary for identifying outliers. Note that the first step is necessary to ensure that the JPDF formulation does not include far-off devices, thus is more robust. Outliers are identified by the quantile that will be determined by the process defectivity rate. These outliers will be dropped and the remaining devices will be used to build the JPDF over the complete set of parameters.

CHAPTER 4. PARAMETER ESTIMATION AND TEST SELECTION

The generic estimation approach can be divided into two parts. The first is the statistical learning phase, and the second is the actual testing phase. The first phase uses the statistical mapping tool to correlate measured parameters to unmeasured parameters, from a small set of training devices. However, defects and outliers cause random behavior which should not be learned because they may corrupt correlation functions. Therefore, the outlier analysis mechanism described in the previous section is used to eliminate these devices from the learning process. With the rest of the test data, the JPDF is built to facilitate the statistical mapping.

During the actual testing phase, not all test data will be available due to the reduction in the number of measurements. The outlier analysis based on these available measurements should provide the same information as the outlier analysis based on all measurements to ensure that defective devices do not escape the testing process. Thus, during test reduction, one has to pay close attention to ensure that all outlier devices are detected with the reduced set of tests. Figure 4.1 illustrates the proposed parameter estimation approach, including the two outlier analysis phases.

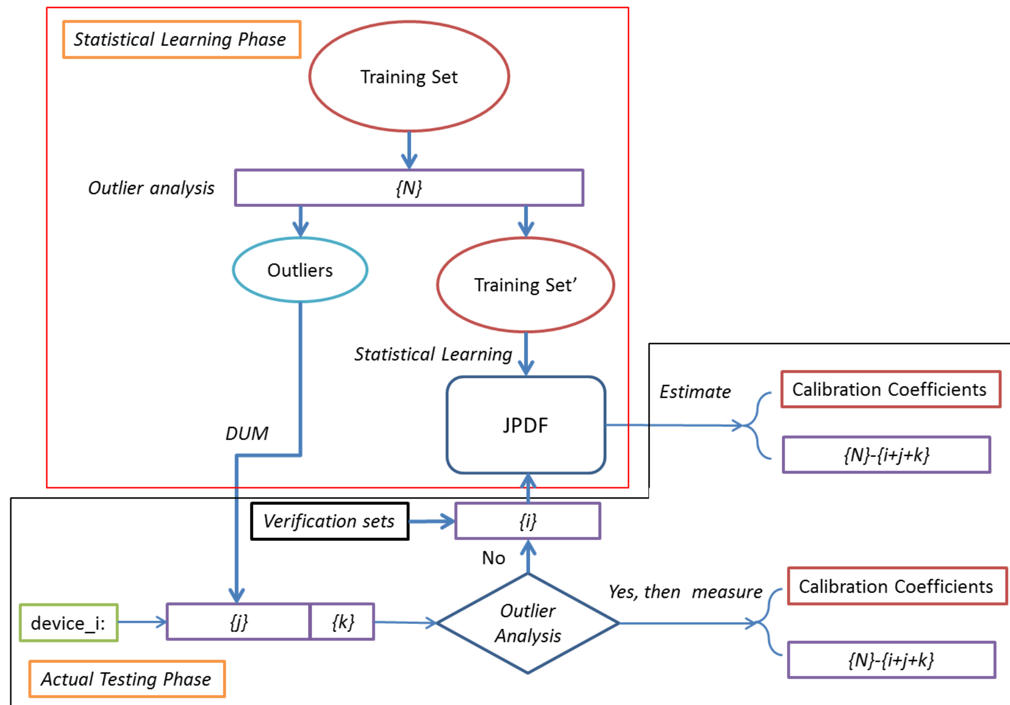

Figure 4.1 Generic estimation test flow

4.1 Statistical Learning Phase

Assume there are *{N}* measurements that need to be tested. During the statistical learning phase, a small number of training devices are selected. These devices are subject to all the tests, including the dynamic wafer-level measurements, and the measurement of calibration coefficients with physical stimuli. Outlier analysis is applied in this phase to prevent learning from defective devices. This phase of the outlier analysis is based on all available

measurements. The final JPDF is built using the remaining samples. The information on extracted outliers is used to determine the reduced set of measurements which can be used for outlier detection in the actual test phase. The flow of the proposed algorithm is presented in section 4.1.1. In addition, from all of the dynamic measurements, those measurements (measurements set *{k}*) which are well correlated to the calibration coefficients, should be selected and applied, in order to accurately estimate the calibration coefficients. This selection can be determined by exploring the mathematical relations of the calibration coefficients. Chapter 6 gives an example of choosing the calibration coefficients of a capacitive accelerometer.

4.1.1 Determining Reduced Set of Tests for Outlier Detection

Ideally, all measurements are available for outlier analysis to prevent defective devices from being shipped. However, as mentioned earlier, this would result in high test times, and would require physical stimulus. In order to reduce the test cost, outlier devices need to be determined with a reduced set of measurements. However, the outcome of this reduced-set outlier analysis needs to be identical (or almost identical) to the outcome of the full-set outlier analysis. An example of using the subset of all measurements to identify outliers is shown in Figure 4.2. Assume there is a sphere located at the origin point with the radius

equal to one. 10,000 instances are evenly distributed inside the sphere except one outlier located at (1, 1, 2). It is obvious that if all elements are projected onto XY plane, the outlier could not be identified. However, the outlier is outstanding at XZ or YZ plane. Hence, either X or Y dimension can be ignored for identifying this outlier.

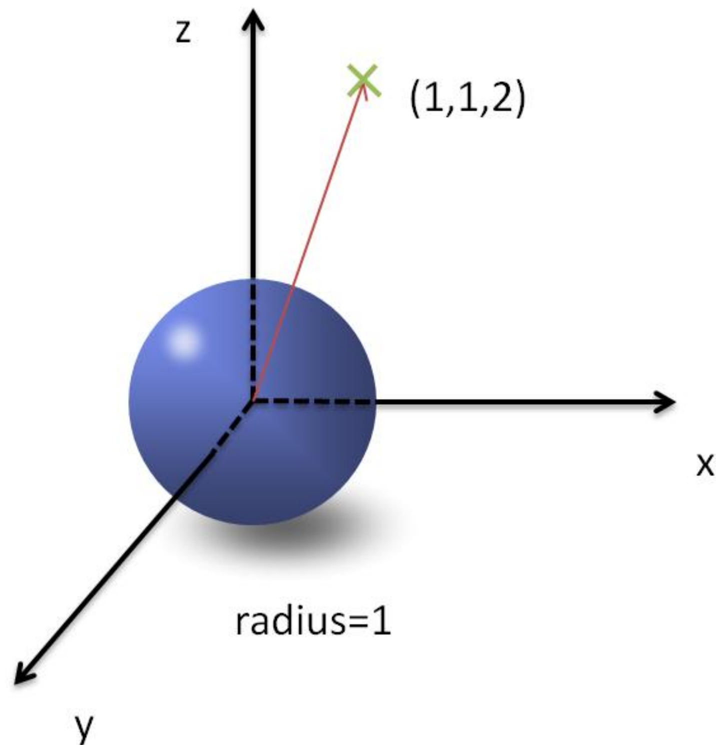

Figure 4.2 Identifying outlier using subset of all dimensions

The algorithm to determine a reduced set of measurements for outlier detection can be explained in the following way. The algorithm utilizes a defined parameter representing the outlier information level called Detection Utility Metric (DUM) [27]. $DUM_{\{j\}}$ is defined as in Equation (4.1.1), where *Threshold* is the outlier identifying boundary, *{j}* is the test list and *{outliers}* are the identified outliers from the training set using the full set of measurements. A heuristic approach is employed to find the most useful tests for outlier detection. First, we order the tests by their *DUM* value over all the detected outliers based on the full set. Then, we select the tests whose *DUM* value is above the given threshold. Out of these tests, we iteratively select and add the tests in the list until the increase of collective *DUM* value falls below 0.001%. This means the rest measurements would not help too much on providing more outlier information. Thus, test list *{j}* is the determined test list for identifying outliers in the actual testing phase.

$$DUM_{\{j\}} = \sum_{\{outliers\}} \sum_{\{j\}} (D_{\{j\}} - Threshold)^2 \qquad (4.1.1)$$

4.2 Selection of Tests to Increase Estimate Accuracy

From the statistical learning phase, the robust outlier free JPDF is constructed, the test list *{k}* is determined for estimating calibration coefficients, and the test list *{j}* is determined for identifying the defective devices. If *device_k*

fails to pass the outlier screening, it will be considered as potentially defective. These devices are either discarded or are subject to more exhaustive testing. If it passes the outlier screening, for the rest tests in this phase, the tests that will be applied need to be carefully selected to achieve a desired estimation accuracy of unmeasured parameters. A subset of the available test data can be considered as the verification set and can be used to select the tests to increase the estimation accuracy. Once again, a heuristic algorithm is used to determine this set of tests.

Assume *device_k* passes the outlier screening *{j}*. In order to select an optimized number and order of the remaining tests, a test re-ordering technique is proposed by applying those tests first, which yields the lowest estimation error of the unmeasured parameters. Specifically, as shown in Figure 4.3, first, we search from the remaining tests and each time we apply a different test to estimate the rest of the measurements. Second, we select the test, which yields the lowest estimation RMS error, and add the test to the test set $\{i\}_{device_k}$,. Third, we continue adding the tests to the test set $\{i\}_{device_k}$, and in the end, a re-ordered test set $\{i\}_{device_k}$ will be generated. It is a test order by ranking tests according to the estimation accuracy of the unmeasured parameters. Since each device may behave slightly different, $\{i\}_{device_k}$ is particular for each device and may not be the same from device to device. Therefore, each device in the verifications sets has its individual test list.

By analyzing all of the individual test lists, we can determine an optimized test set (test list $\{i\}$) for the verification sets. We apply different numbers of tests and estimate the rest tests. For a certain number (N) of tests we apply, the test order can be determined by selecting the top N frequently appearing tests in all the top N tests of the individual test lists $\{i\}_{device_k}$.

In the end, each verification set can generate the estimation error of a different number of tests. Moreover, for all the verification sets, the consistency of the estimation error will be analyzed, to verify the robustness and the reliability of the verification set size. A robust and reliable verification set size for several sets should provide the same general test list, the similar level of estimation error and the similar variation trend of the estimation error. Therefore, for the actual testing devices, the verified general test list is robust and reliable to achieve the optimized estimation accuracy.

```
Algorithm:

{i} ={}
for  verification sets=1:N
        for  device_k=1:M
                if  device_k  passed outlier check
                        for test#=1:size(rest tests)
                                for {m}=1:rest tests
                                        RMS_{m}
                                end
                                {m}= min(RMS_{m})
                                {i} ={i} +{m}
                                update rest tests
                        end
                else apply full test
        end
end
```

Figure 4.3 Algorithm for finding test list *{i}*

CHAPTER 5. CASE STUDY: ACCELEROMETER

In this chapter, dynamic measurements for estimating the accelerometer calibration coefficient are determined. After outlier screening, an estimation process is presented and analyzed based on simulations using a generic capacitive accelerometer model in MATLAB.

5.1 Determining Dynamic Accelerometer Measurements for Correlating to Calibration Coefficients

Due to process variations, each particular MEMS device might produce different output under a reference input stimulus. The Calibration Coefficient (CC) is a parameter used for calibrating each particular device output to a reference output. For a capacitive accelerometer, as shown in Figure 1.1 and Figure 1.2, the dynamic capacitance difference $\Delta C_{dynamic}$ is the parameter that is measured to convert the acceleration to an electrical response. The definition of the calibration coefficient is shown in equation (5.1.1)

$$CC = \frac{\Delta C_{dynamic} - \Delta C_{offset}}{\Delta C_{dynamic_nom}} \quad (5.1.1)$$

where ΔC_{offset} , $\Delta C_{dynamic}$ and $\Delta C_{dynamic_nom}$ are defined as:

$$\Delta C_{offset} = C1 - C2 = \xi * \xi_o * A * \left(\frac{1}{Gap_a} - \frac{1}{Gap_b}\right) \quad (5.1.2)$$

$$\Delta C_{dynamic} = \xi * \xi_O * A * (\frac{1}{Gap_a - \frac{a*m}{k}} - \frac{1}{Gap_b + \frac{a*m}{k}}) \quad (5.1.3)$$

$$\Delta C_{dynamic_nom} = \xi * \xi_O * A_{_nom} * (\frac{1}{Gap_{_nom} - \frac{a*m_{_nom}}{k_{_nom}}} - \frac{1}{Gap_{_nom} + \frac{a*m_{_nom}}{k_{_nom}}}) \quad (5.1.4)$$

In equations (5.1.2), (5.1.3) and (5.1.4), A is the capacitance area. Gap_a and Gap_b are the distance between two fingers. m , k are mass and spring constant respectively. m , k , A , ξ , Gap are five process variables and $\Delta C_{dynamic_nom}$ is the capacitance when all process variables are the nominal values. To simplify the equations of calibration coefficient and better observe the correlated dynamic measurements, first order analysis reveals small displacement x, which is linearly related to ΔC (Equation (5.1.5) - (5.1.7)).

$$C_2 - C_1 = 2\Delta C = 2\xi_o \xi \frac{x}{Gap^2 - x^2} \quad (5.1.5)$$

$$\Delta C x^2 + \xi_o \xi A x - \Delta C * Gap^2 = 0 \quad (5.1.6)$$

$$x \approx \frac{Gap^2}{\xi \xi_o} \Delta C \quad (5.1.7)$$

Hence, the calibration coefficient can be simplified as:

$$CC = \frac{\Delta C_{dynamic} - \Delta C_{offset}}{\Delta C_{dynamic_nom}} = \frac{\xi A}{\xi_{_nom} A_{_nom}} * \frac{m}{m_{_nom}} * \frac{k_{_nom}}{k} = \frac{\xi A}{\xi_{_nom} A_{_nom}} * \frac{{f_{R_nom}}^2}{{f_R}^2} \quad (5.1.8)$$

where CC is independent to input acceleration and highly correlated to dielectric constant, capacitance area, proof mass and spring constant.

In order to accurately estimate the calibration coefficient, it is necessary to select dynamic measurements that correlate well with these five process variables. Since the spring-mass system is a second-order system, it presents with a resonance frequency (f_R), which is highly correlated to the spring constant and the mass. Moreover, the static capacitances that the device presents when there is no movement (C_1 and C_2) are related to the area of the fingers, the gap between the fingers, and the electrostatic constant of the dielectric material between the fingers. Thus, these three parameters contain all the ingredients necessary to establish the correlations that we wish to obtain.

f_R , C_1 and C_2, are defined as in equation (5.1.9) -(5.1.11),

$$f_R = \sqrt{\frac{k}{m}} * \frac{1}{2\pi} \tag{5.1.9}$$

$$C_1 = \xi * \xi_o * A * \frac{1}{Gap_a} \tag{5.1.10}$$

$$C_2 = \xi * \xi_o * A * \frac{1}{Gap_b} \tag{5.1.11}$$

Figure 5.1 shows the complete estimation test flow including outlier analysis. After training set compaction for building robust JPDF, device_i goes through the tests of f_R , C_1 and C_2. If it passes outlier screening, its calibration coefficient will be estimated according to the JPDF.

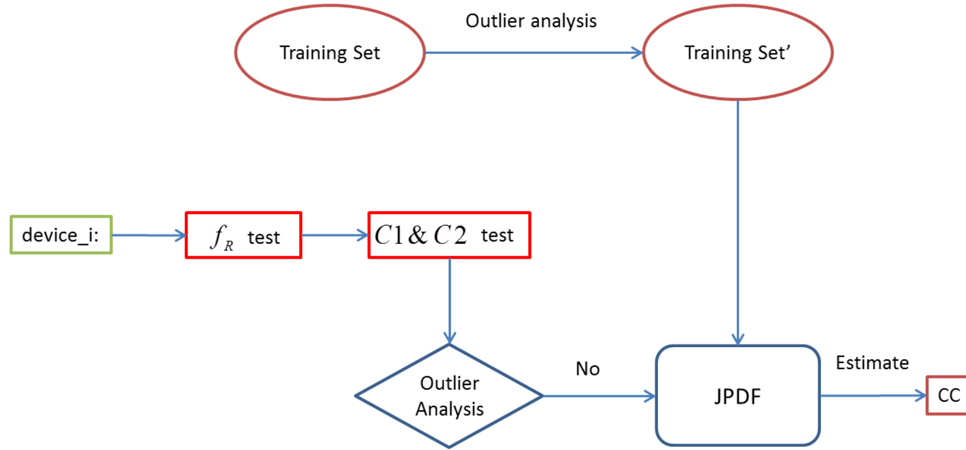

Figure 5.1 Complete estimation test flow

5.2 Simulation Results

In order to evaluate the effectiveness of the outlier analysis technique, a MATLAB model for the accelerometer is used to generate simulation data. Outliers are intentionally added to generate a diverse set of samples. (1000 of samples are used within process variations as defined by a reference MEMS process (information provided by Freescale Corp.) In addition, 100 samples are added at the 6-8 sigma range as outliers.

Out of this set of 1100 sample devices (1000 devices with process variations and 100 devices as outliers), we select half of them to train the learning process. As such, there are roughly 50 outlier devices in this training set. The histogram of the distances (Equation 3.2.2 and Equation 3.2.3) associated with

this training set is shown in Figure 5.2. In this specific example, we know that roughly 10% of devices are defective (outliers), thus we can set the threshold for the quantile accordingly. In an industry setting, estimates for defect rates can be used to set this threshold. This defect rate metric does not need to be very accurate; it needs to represent roughly what percentage of devices might be defective. Comparing these selected outliers by the technique with the actual defects injected, we find out that 50 (100%) intentionally added outliers in the verification set are identified as the outliers.

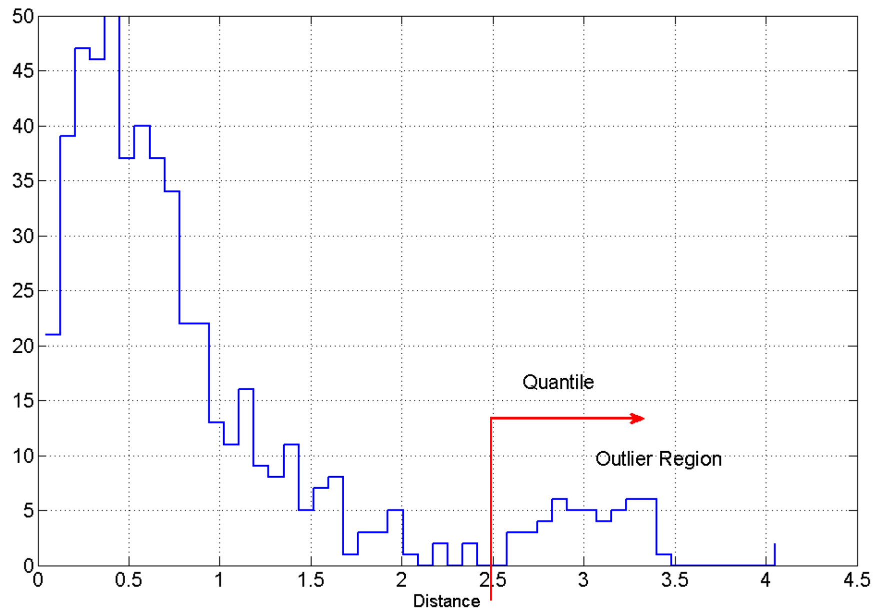

Figure 5.2 Training set distance histogram plot

Estimation of calibration coefficient

Once the JPDF is established using the training set after pruning the outliers away, we evaluate the technique to estimate the calibration coefficients for the remaining 550 devices. 50 outliers of those 550 devices can be detected to avoid reduction of estimation accuracy. The rest of the 500 normal devices can be evaluated to estimate the calibration coefficient.

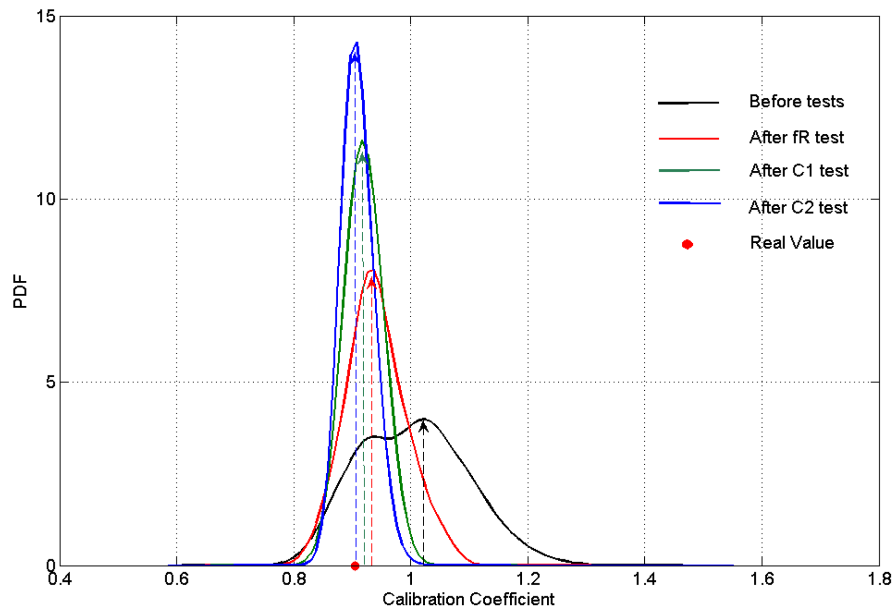

Figure 5.3 Calibration Coefficient is localized after 2 tests

For a sample device, Figure 5.3 demonstrates how the calibration coefficient distribution is localized after three tests. The most likely value of the calibration coefficient is 1.1, as this corresponds to the nominal value. After three

tests, the blue curve shows the new span of the calibration coefficient. The most likely value is 0.905 whereas the actual value of the parameter corresponds to 0.907. Thus, using this estimation technique, the calibration coefficient is determined within 0.3% of its actual value. Similarly, the error has reduced from 21% to 0.3%.

In order to demonstrate that the estimation can be done accurately across a large number of devices, we have used the errors associated with all the 500 estimations from the verification set. Figure 5.4 illustrates scatter plot of the actual and the estimated value. Ideally, if there is no estimation error, this plot would be a straight line with the slope equal to 1, as the red dashed line shown in these two figures.

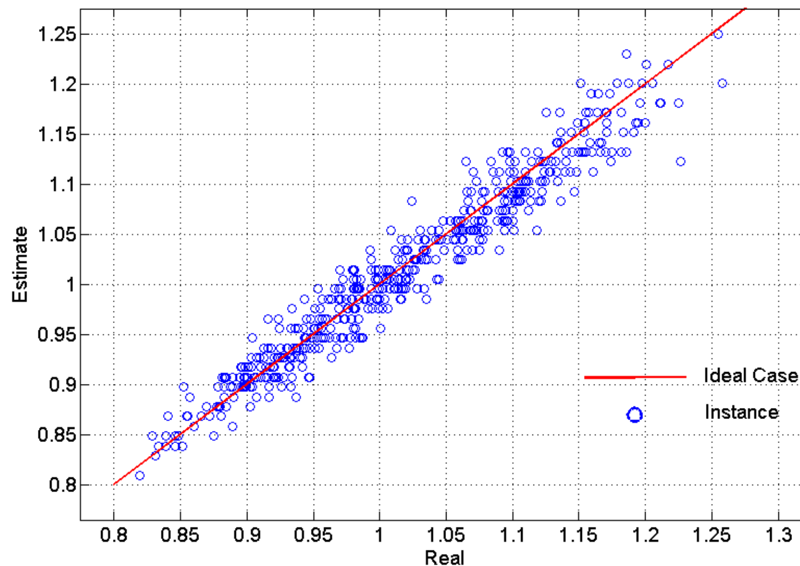

Figure 5.4 Scatter plot of Real vs Estimate after all tests

The figure shows that there is very good correlation between the actual and estimated values of the calibration coefficients across a wide range of process variations.

As a further metric for evaluation, we use the RMS error across these samples. The RMS error is defined as equation (5.1.7):

$$RMS = \sqrt{\frac{1}{N}\sum_{N}\left(\frac{real - estimate}{real}\right)^2} \tag{5.1.7}$$

where N is the number of devices in the verification set.

Table 5.1 shows the impact of training set size on the estimation accuracy. It is shown clearly that the larger the training size, the better the estimation accuracy. The reason is obvious: larger training sets provide more robust, complete and precise statistical correlations.

Training set size	RMS before tests	RMS after f_R test	RMS after C1 test	RMS after C2 test
500	0.0913	0.0505	0.0319	0.0211
400	0.0905	0.0519	0.0321	0.0229
300	0.0900	0.0533	0.0332	0.0240
200	0.0894	0.0555	0.0341	0.0255
100	0.0905	0.0582	0.0368	0.0310

Table 5.1 RMS errors after each test with different training size

CHAPTER 6. A CASE STUDY: GYROSCOPE

In this chapter, we present results on wafer-level test reduction for a gyroscope using industry-provided data. We show that (a) outlier devices can be effectively identified with the reduced set, and (b) the remaining wafer-level test parameters can be accurately determined from the measured set using the statistical mapping tool.

The data on the gyroscope are provided by Freescale Corp. These data include 23 dynamic measurements on various resonant frequencies, damping coefficients, and other frequency-related characteristics. These measurements are conducted by applying a stimulus that is close to the unknown resonant frequency, stopping the excitation, and observing the device's response after the excitation has been stopped. The behavior is analyzed in the frequency domain using signal processing techniques. All measurements are conducted near 2kHz over about half a second. Thus, the overall test time can be roughly estimated as 10 seconds, which is deemed to be very long for this device.

6.1 Outlier Analysis on Full Set of Measurements

Figure 6.1 presents the percentage of outliers versus index of simulations, where the total device number is 2741. Each of 14 simulations was run by

randomly selecting training devices in order to prove the high stability of kernel based outlier analysis. The training set is built from half of all devices and training set distance boundary is set as 99% quantile. It is clearly shown in the figure that outlier proportion is firmly stable at about 2X% (actual numbers are obscured to hide sensitive yield information). Training set size impact is revealed in Table 6.1, which proves the insensitivity of training set size.

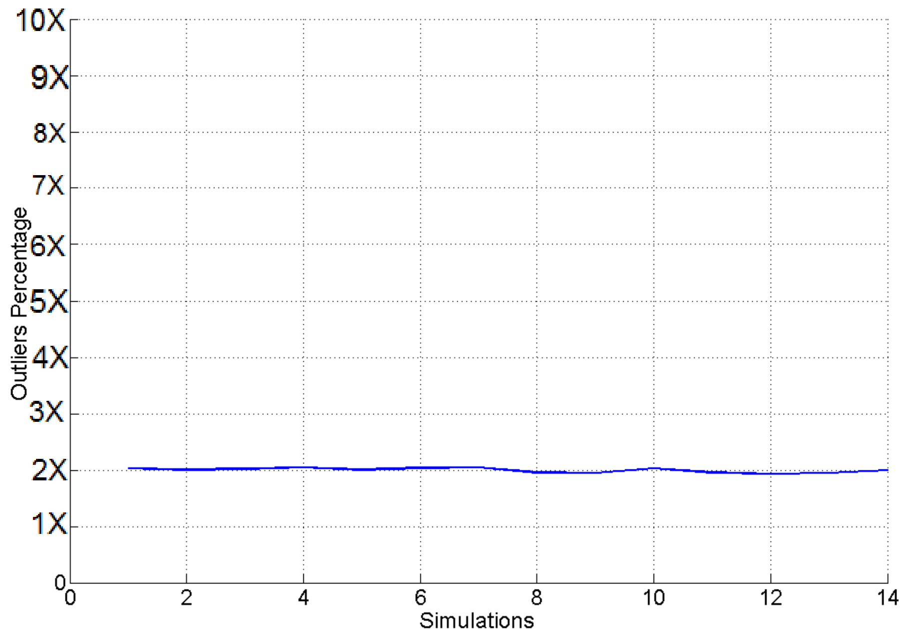

Figure 6.1 Outlier percentage *vs* index of simulations

Training set size	Identifying outliers #
400 (14.6%)	N (X %)
700 (25.5%)	N+18 (X+0.656 %)
1000 (36.5%)	N-12 (X-0.439 %)
1370 (half)	N-26 (X-1.314 %)

Table 6.1 Training set size impact on outlier identifying

6.2 Outlier Analysis based on Subset of Measurements

Experimental results show 10 tests can be used for identifying outliers. Table 6.2 indicates the effectiveness of using a reduced set of measurements for identifying outliers. The selection of 25% of all instances as the training set, misses less than 1% outliers using the subset of all dimensions.

Training set size	Identifying outliers # (all dimensions)	Identifying outliers # (subset of all dimensions)	Match (%)
400 (14.6%)	X	X-18	96.853%
700 (25.5%)	X+18	X+13	99.153%
1000 (36.5%)	X-12	X-13	99.821%
1370 (half)	X-26	X-27	99.813%

Table 6.2 Training set size impact on identifying outliers not using all dimensions

6. 3 Verification sets consistency analysis

Figure 6.2 shows the averaging RMS errors of four different verification sets after different numbers of tests. From the consistency point of view, all four verification sets indicate that the estimation error is reduced considerably after four tests and fluctuates unpredictably after the reduction. Hence, the optimized selection is to choose four tests. In addition, the estimation errors of four sets by

four tests are 1.087, 0.9233, 0.3299 and 0.9220 respectively. Therefore, the estimated error level is obtained, which is from 0.3 to 1.1.

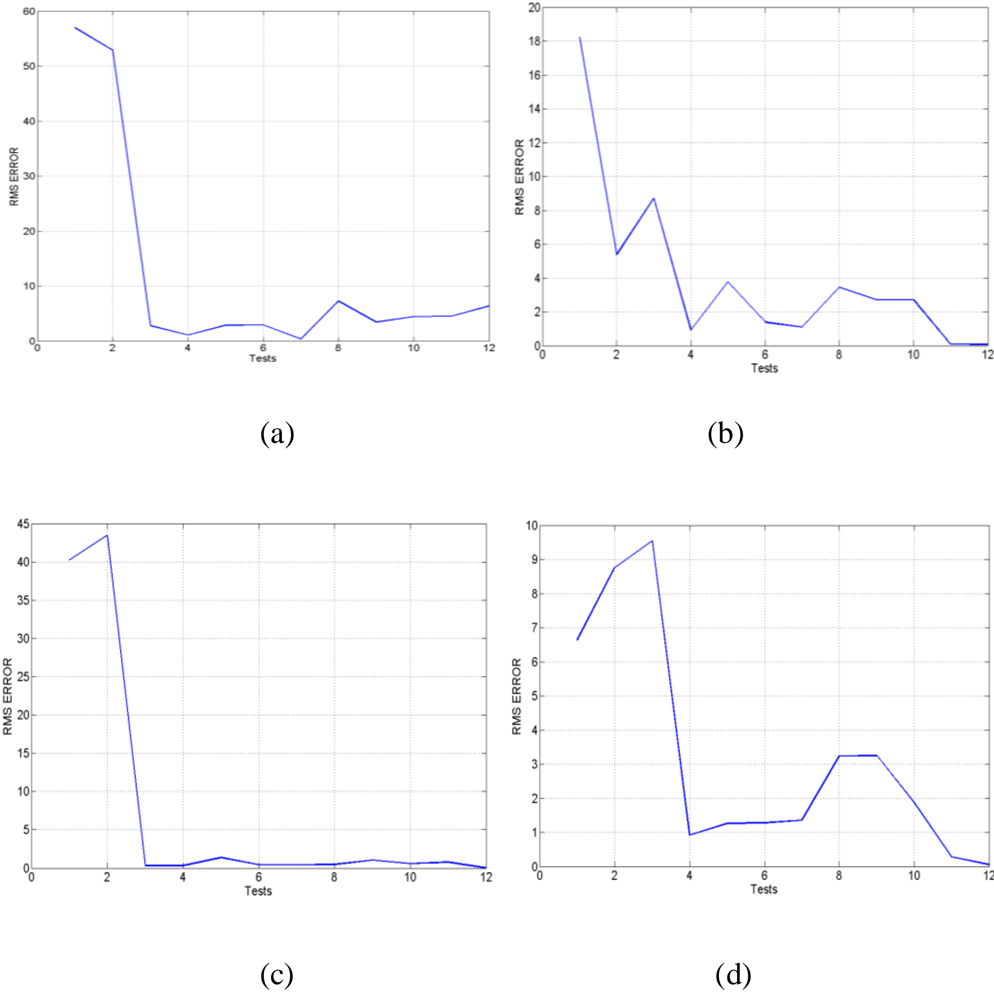

Figure 6.2 Average RMS errors after different number of tests for 4 different verification set (a), (b), (c), (d)

6.4 Experimental Results of Estimation Process

Figure 6.3 reveals estimation RMS errors by adding different a number of tests for all devices outside the training set. It proves the effectiveness of test list determination algorithm by verification sets. Significant reduction in estimation error can be observed after four tests, followed by a random fluctuation. The estimation error of four tests is 0.7800, which is between the section of estimated error level. We also show that the outlier analysis is absolutely necessary before statistical learning. Table 6.3 compares the estimation errors when the statistical learning phase includes an outlier analysis to the estimation errors without an outlier screening. Independent of the training set size, outlier screening is essential to ensure that the estimation can be done accurately.

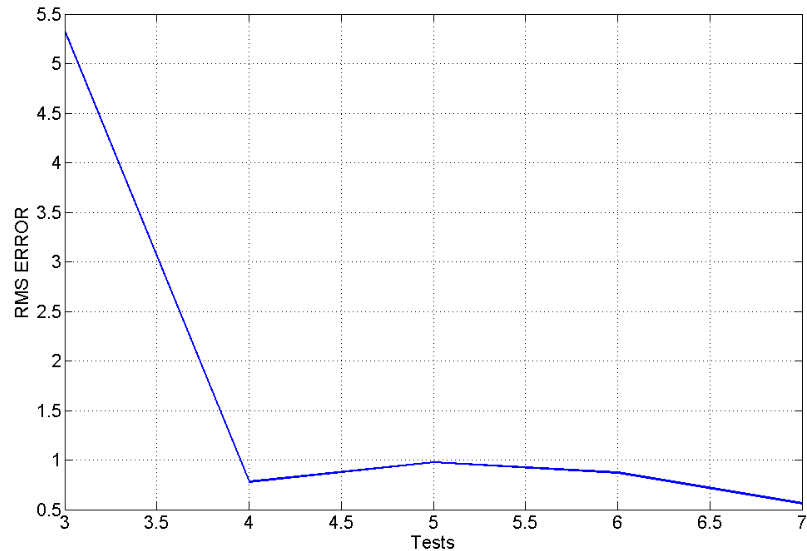

Figure 6.3 Experimental results of RMS errors using different number of tests

Training set	After outlier screen	Before outlier screen
	RMS	RMS
300 (13.6%)	2.1516	43.937
500	1.1139	39.761
700	1.0804	32.265
900	1.0427	30.267
1100 (50%)	0.7800	23.780

Table 6.3 Improvement on estimation accuracy after outlier screening

Figure 6.4 demonstrates how one of measurements is localized after the device goes through the whole test list. The X axis stands for test index. As shown in this figure, there are fourteen measurements on the test list. Y axis is the error percentage, where the red line represents the real value and each vertical blue line stands for three sigma error range. The middle of each vertical blue line is the mean values and connected to show how it varies during tests. We can observe that measurement 10 is widely distributed, but after several tests it is almost localized to real value with narrow distribution. The original estimation error is 51%; three sigma ranging around 200%. After all of the measurements, the estimation error decreases by 17%, improving over 100% and three-sigma ranges around 1%. Figure 6.5 shows how all measurements are localized for one device.

It is apparent that almost all of the measurements are accurately localized to real value with little error.

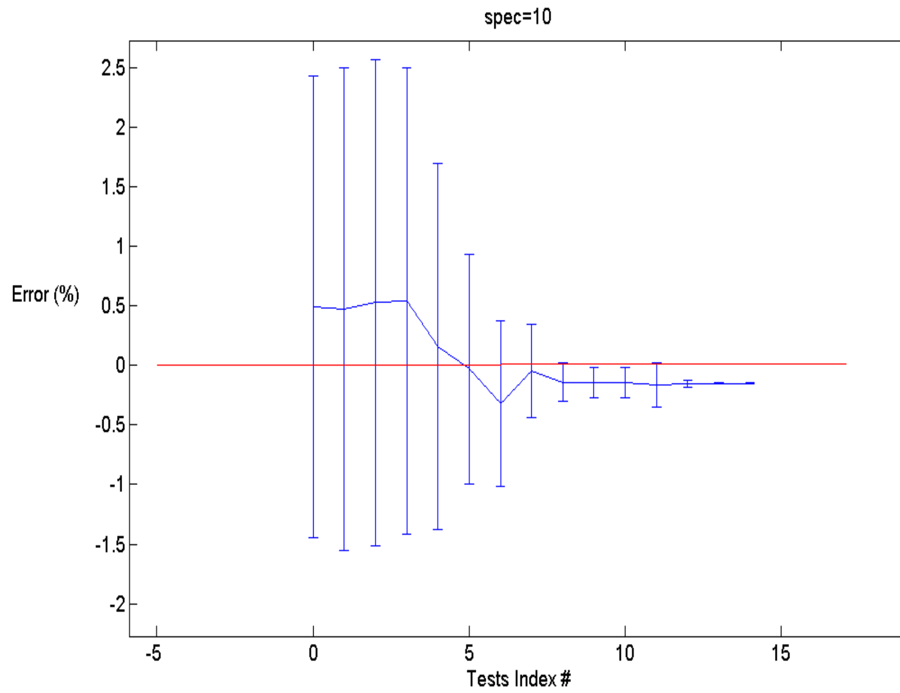

Figure 6.4 Measurement ten is localized after tests on whole test list

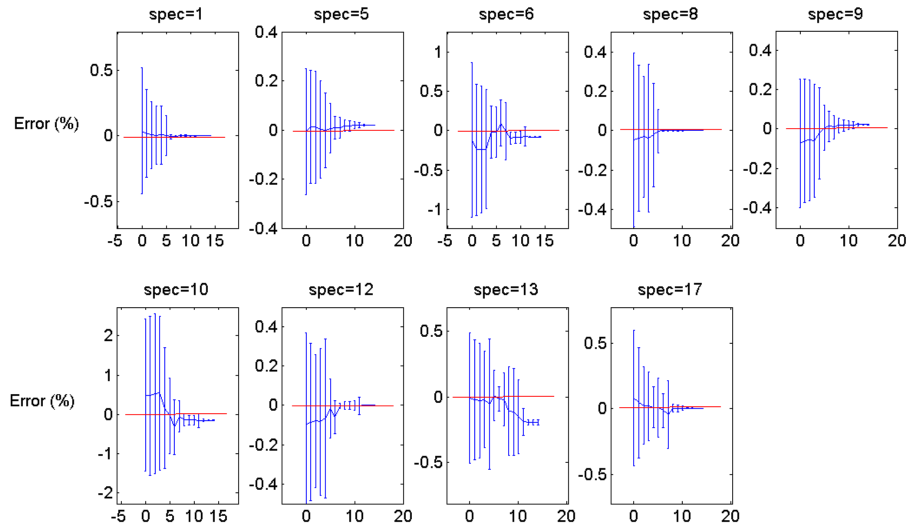

Figure 6.5 Estimated measurements are localized after all of the tests

Figure 6.6 presents experimental results of the worst and the best estimated devices. The red line is the zero error line. The blue line is the mean-value-error path of the best device while the black line is that of the worst device. Almost all of the estimation errors of the best and worst estimated device are below 5%, except one measurement of the best has 20% error; two measurements of the worst have the error of 60% and 28%.

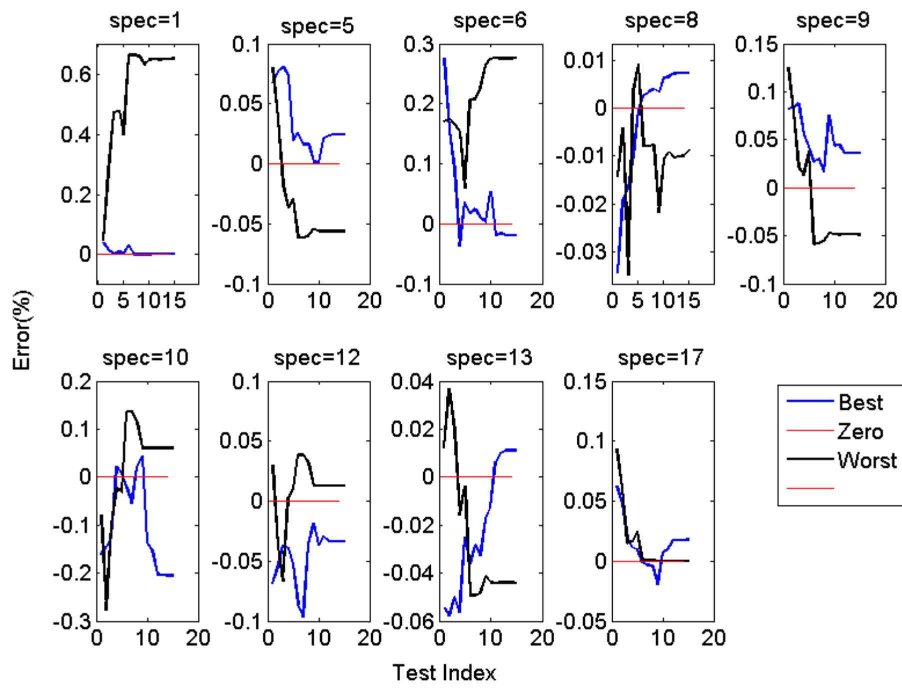

Figure 6.6 Worst and best estimated devices during prediction process

CHAPTER 5. CONCLUSION AND FUTURE WORK

Utilizing electrostatic force generating from comb-drive fingers is the main idea of electrically exciting MEMS capacitive accelerometer and gyroscope. Resonant frequency and stationary capacitance can be utilized to estimate the calibration coefficient for accelerometer, without using physical stimulus. Kernel based statistical model has proved to be an effective and accurate tool for identifying multi-D outliers while having a reasonable estimation accuracy. The accelerometer analysis proved the effectiveness for low dimensions, while gyroscope analysis proved the effectiveness for high dimension. Subset of all measurements is proved to be effective and accurate for outlier analysis. For high dimension estimation process and from experimental results, outlier screening greatly improves estimation accuracy. Some small sets of verification devices can be employed to generate an optimized general test list with decent test time reduction and prediction accuracy. In addition, an estimated prediction error can be achieved by verification sets.

Future works may concentrate on test quality control. It is necessary to select a larger training set to robust statistics if the measurements have low correlations. Test quality control mechanism would be considered in order to select decent training set size. Measurement error is not considered in this thesis,

and it may affect test quality. Consistency analysis of several verification sets can provide confidence and controlled accuracy for test list determination to some extent, but future improvement may be required on this topic. From device point of view, each type of MEMS sensor may suffer from different sorts of defects such as stiction, curvature, etch variation, particular contamination, etc. Each defect may influence several measurements. Defects screening might emphasize those measurements. Algorithms that optimize the test list might make an improvement on estimation accuracy.

- Summary of contributions
  - Determine electrical based measurements of accelerometer for predicting calibration coefficient
  - Training set outlier screening mechanism to build a robust statistical JPDF for prediction process
  - Include outlier screening mechanism into test flow to improve prediction accuracy
  - Algorithm for determining and optimizing estimation test list
  - Predictable estimate error provided by determining and optimizing test list process

REFERENCE

[1] Ultimate MEMS market Analysis, April 2005
(http://www.the-infoshop.com/study/yd27263_mems.html)

[2] J. Marek, "Automotive MEMS sensors — Trends and applications", *International Symposium on*, pp. 1-2, 2011.

[3] L. S. Fan, Y. C. Tai and R. S. Muller, "IC-processed electrostatic micro-motors", *IEEE International Electron Devices Meeting,* pp. 666-669, 1988.

[4] Baltes, O. Brand, G. K. Fedder, C. Hierold, J. Korvink and O.Tabata, "CMOSMEMS: Advanced Micro and Nanosystems", Wiley-VCH, 2005.

[5] Piezoelectric multilayer triaxial accelerometer
(http://www.noliac.com/Files/Billeder/11%20Publications/Piezoelectric_multilayer_triaxial_accelerometer.pdf)

[6] Mikko Saukoski, "System And Circuit Design For A Capacitive MEMS Gyroscope", Doctoral Dissertation, Helsinki University of Technology, 2008.

[7] T.C. Lu, Y.J. Huang, and H.P. Chou, "A novel interface circuit for capacitive sensors using correlated double sampling demodulation technique", *Second International Conference on Sensor Technologies and Application*, pp. 396-400, August 2008.

[8] B. V. Amini and F. Ayazi, "A 2.5 V 14-bit Sigma-Delta CMOS SOI Capacitive Accelerometer", *IEEE J. Solid-State Circuits*, vol-39, No. 12, pp. 2467-2476, 2004.

[9] A. Kolpekwar, and R.D. Blanton, "Development of a MEMS testing methodology", *International Test Conference,* pp. 923-931, 1997.

[10] H.G Kerkhoff, "Testing of MEMS-based microsystems", *European Test Symposium,* pp. 223- 228, 2005.

[11] S. Mir, and B. Charlot, "On the integration of design and test for chips embedding MEMS", *IEEE Design & Test of Computers,* vol. 16, no. 4, pp. 28-38, 1999.

[12] B.Charlot, S. Mir, F. Parrain, and B. Courtois, "Electrically induced stimuli for MEMS self-test", *IEEE VLSI Test Symposium,* pp. 210-215, 2001.

[13] X. Xiong, Y. Wu, and W.-B. Jone, "A dual-mode built-in self-test technique for capacitive MEMS devices", *IEEE Transactions on Instruments and Measurements*, vol. 54, no. 5, pp. 1739- 1750, 2005.

[14] M.F. Islam, and M.A.M. Ali, "On the use of a Mixed-Mode Approach For MEMS Testing", *IEEE International Conference,* pp. 62-65, 2006.

[15] L. Rufer, S. Mir, E. Simeu, and C. Domingues, "On-chip testing of MEMS using pseudo-random test sequences", *IEEE conference symposium*, pp. 50- 55, 2003.

[16] L. Ciganda, P. Bernardi, M.S. Reorda, D. Barbieri, M. Straiotto, and L. Bonaria, "A tester architecture suitable for MEMS calibration and testing", *IEEE International Conference*, pp. 1, 2010.

[17] R. O'Reilly, H. Tang and W. Chen, "High-g testing of MEMS devices, and why", *IEEE Sensors*, pp. 148-151, 2008.

[18] H. Zhang, J. Zhao, X. Zhou, and H. Jiang, "A New Test Method and System of Low-cost MEMS Gyroscope", *International Conference on Electronic Measurement and Instruments,* pp. 4-307-4-310, 2007.

[19] S. Biswas, L. Peng, R.D. Blanton, and L.T. Pileggi, "Specification test compaction for analog circuits and MEMS [accelerometer and opamp examples]", *IEEE Design, Automation and Test in Europe*, Vol. 1, pp. 164- 169, 2005.

[20] V. Natarajan, S. Bhattacharya, and A. Chatterjee, "Alternate electrical tests for extracting mechanical parameters of MEMS accelerometer sensors", *IEEE VLSI Test Symposium,* pp. 6, 2006.

[21] A.A. Rekik, F. Azais, N. Dumas, F. Mailly, and P. Nouet, "Investigations on electrical-only test setup for MEMS convective accelerometer", *International Conference on Signals, Circuits and Systems (SCS),* pp. 1-6, 2009.

[22] A.A. Rekik, F. Azaïs, N. Dumas, F. Mailly, and P. Nouet, "An electrical test method for MEMS convective accelerometers: Development and evaluation", *Europe Conference & Exhibition*, pp. 1-6, 2011.

[23] A.A. Rekik, F. Azais, N. Dumas, F. Mailly, and P. Nouet, "Test and calibration of MEMS convective accelerometers with a fully electrical setup", *Latin American Test Workshop,* pp. 1-6, 2011.

[24] V. Litovski, M. Andrejevic, and M. Zwolinski, "ANN based modeling, testing and diagnosis of MEMS [capacitive pressure transducer example]," *7th Seminar on Neural Network Applications in Electrical Engineering,* pp. 183- 188, 2004.

[25] N. Dumas, F. Azais, F. Mailly, P. Nouet, "Evaluation of a fully electrical test and calibration method for MEMS capacitive accelerometers," *IEEE International Mixed-Signals, Sensors, and Systems Test Workshop,* pp. 1-6, 2008.

[26] E. Yilmaz and S. Ozev, “Adaptive test flow for mixed-signal/RF circuits using learned information from device under test,” *IEEE International Test Conference*, pp. 1–10, 2010.

[27] Ender Yilmaz and Sule Ozev, “Adaptive Multidimensional Outlier Analysis for Analog and Mixed Signal Circuits,” *IEEE International Test Conference,* pp. 10-2, 2011.